

## Article (refereed) - postprint

---

Miller, James D.; Grebby, Stephen. 2014. **Mapping long-term temporal change in imperviousness using topographic maps.**

© 2014 Elsevier B.V.

This version available <http://nora.nerc.ac.uk/505474/>

NERC has developed NORA to enable users to access research outputs wholly or partially funded by NERC. Copyright and other rights for material on this site are retained by the rights owners. Users should read the terms and conditions of use of this material at <http://nora.nerc.ac.uk/policies.html#access>

NOTICE: this is the author's version of a work that was accepted for publication in *International Journal of Applied Earth Observation and Geoinformation*. Changes resulting from the publishing process, such as peer review, editing, corrections, structural formatting, and other quality control mechanisms may not be reflected in this document. Changes may have been made to this work since it was submitted for publication. A definitive version was subsequently published in *International Journal of Applied Earth Observation and Geoinformation*, 30. 9-20. [10.1016/j.jag.2014.01.002](https://doi.org/10.1016/j.jag.2014.01.002).

[www.elsevier.com/](http://www.elsevier.com/)

Contact CEH NORA team at  
[noraceh@ceh.ac.uk](mailto:noraceh@ceh.ac.uk)



22 **Abstract**

23 Change in urban land use and impervious surface cover are valuable sources of information for  
24 determining the environmental impacts of urban development. However, our understanding of  
25 these impacts is limited due to the general lack of historical data beyond the last few decades.  
26 This study presents two methodologies for mapping and revealing long-term change in urban  
27 land use and imperviousness from topographic maps. Method 1 involves the generation of maps  
28 of fractional impervious surface for direct computation of catchment-level imperviousness.  
29 Method 2 generates maps of urban land use for subsequent computation of estimates of  
30 catchment imperviousness based on an urban extent index. Both methods are applied to estimate  
31 change in catchment imperviousness in a town in the South of England, at decadal intervals for  
32 the period 1960–2010. The performance of each method is assessed using contemporary  
33 reference data obtained from aerial photographs, with the results indicating that both methods are  
34 capable of provide good estimates of catchment imperviousness. Both methods reveal that peri-  
35 urban developments within the study area were demonstrated to have undergone a significant  
36 expansion of impervious cover over the period 1960–2010, which is likely to have resulted in  
37 changes to the hydrological response of the previously rural areas. Overall, results of this study  
38 suggest that topographic maps provide a useful source for determining long-term change in  
39 imperviousness in the absence of suitable data, such as remotely sensed imagery. Potential  
40 applications of the two methods presented here include hydrological modelling, environmental  
41 investigations and urban planning.

42

43

44

## 45 **1. Introduction**

46 Accurate estimates of impervious surface coverage (commonly known as  
47 imperviousness) within watersheds (catchments) are required for hydrological modelling and  
48 urban land use planning because increased imperviousness results in decreases in infiltration and  
49 soil storage capacities (Kidd & Lowing, 1979). Furthermore, replacement of natural drainage  
50 with artificial conveyance pathways can also reduce catchment response times (Packman, 1980).  
51 These impacts can subsequently combine to increase the frequency and magnitude of flood  
52 events through increased and more rapid runoff (Huang et al., 2008; Villarini et al., 2009), and  
53 lead to disruption of natural groundwater recharge (Shuster et al., 2005; Im et al., 2012).  
54 Moreover, the hydrological alterations caused by increasing imperviousness typically give rise to  
55 environmental issues, such as degraded water quality, decreased biodiversity in water bodies,  
56 and increased stream-bank erosion (Schueler, 1994; Arnold & Gibbons, 1996; Hurd & Civco,  
57 2004; Amirsalari et al., 2013). Such impacts can be especially pronounced in peri-urban  
58 developments; areas surrounding existing towns, which convert previously permeable rural land  
59 into highly impermeable and artificially drained catchments (Tavares et al., 2012).

60 Understanding and modelling the long-term hydrological impacts of increased urban  
61 development requires concurrent information on the change in impervious surface coverage.  
62 Maps of impervious surfaces can be produced from either field surveys, manually digitising from  
63 hard-copy topographic maps, or the use of remote sensing (RS) data. Whereas field surveys and  
64 manual digitisation can be time-consuming and laborious, the large continuous areal coverage  
65 provided by RS datasets can be exploited using image processing algorithms to rapidly map  
66 impervious surfaces for only a fraction of the time and cost. Accordingly, RS is becoming  
67 increasingly recognised as a valuable tool for mapping imperviousness.

68 A comprehensive, authoritative review of the different methodologies employed to map  
69 impervious cover from RS data is provided by Weng (2012). To summarise, RS-based  
70 approaches to mapping imperviousness generally fall into three broad categories: per-pixel,  
71 object-based and sub-pixel. Per-pixel approaches commonly involve producing a binary map by  
72 determining whether individual image pixels correspond to either pervious or impervious  
73 surfaces, typically through aggregating the classes of an initial land cover classification (Yuan &  
74 Bauer, 2006; Im et al., 2012; Amirsalari et al., 2013). In contrast, object-based approaches  
75 involved the classification of groups of contiguous image pixels (i.e., objects or regions) by also  
76 considering various shape, contextual and neighbourhood information (Benz et al., 2004; Weng,  
77 2012). Classifying an image based on objects helps to overcome the “speckled” effect often  
78 encountered with per-pixel classification in urban areas (Van de Voorde et al., 2003), thus  
79 enabling improved mapping results (Yuan & Bauer, 2006; Zhou & Wang, 2008). A major  
80 limitation of per-pixel approaches is that they assume each pixel comprises a single land use or  
81 land cover type. However, pixels containing a mixture of land use or cover types are common in  
82 low-to-moderate resolution imagery acquired over complex heterogeneous landscapes such as  
83 urban areas (Weng, 2012). Sub-pixel approaches can be used to overcome this to derive accurate  
84 estimates of imperviousness because they decompose the pixel spectra into their constituent  
85 parts, therefore providing fractional measures of impervious surface area. Popular approaches in  
86 this category include unmixing the pixel spectra to determine the fractional abundance of each  
87 constituent end-member surface type (Wu & Murray, 2003; Lu et al., 2006), or modelling  
88 fractional imperviousness through statistical regression and scaling of spectral vegetation indices  
89 (Carlson & Arthur, 2000; Gillies et al., 2003; Bauer et al., 2004; Van de Voorde et al., 2011).

90           With the earliest source of RS data comprising panchromatic aerial photograph lacking in  
91 sufficient spectral information, the mapping of imperviousness using RS is restricted to the last  
92 few decades since the emergence of spectral satellite imagery (e.g., Landsat). Consequently, few  
93 studies have assessed long-term land cover change using RS data (e.g., Gerard et al., 2010;  
94 Tavares et al., 2012), and even fewer have mapped long-term changes in impervious cover  
95 (Weng, 2012). Therefore, our understanding of the hydrological impact and non-stationary  
96 flooding trends in relation to impervious surface change is somewhat limited (Ogden et al., 2011;  
97 Vogel et al., 2011; Dams et al., 2013).

98           Linking imperviousness to alternative sources of digital geo-information could provide a  
99 means of mapping long-term changes in impervious cover. However, such datasets are not  
100 usually available at the national scale or comparable over long periods of time. National land  
101 cover mapping products such as the UK Land Cover Map (LCM) 1990, 2000 and 2007 (Centre  
102 for Ecology and Hydrology) cover only a short time period and are inconsistent due to the  
103 different processing algorithms applied to derive each product from the RS data (Morton et al.,  
104 2011). While methods such as land use trajectory analysis (Verbeiren et al. 2013) could be  
105 applied to help improve the consistency of the time-series somewhat, there will still likely be a  
106 residual error arising from the use of contrasting algorithms for generating each data product.  
107 Physical settlement boundaries and land use change statistics may be a useful alternative source  
108 of information (e.g., Bibby, 2009) but can only be loosely regarded as proxies for  
109 imperviousness. In most cases, the only consistent and long-term sources are topographic maps  
110 produced by national agencies. Within the UK topographic maps have been produced by the  
111 Ordnance Survey — the national mapping agency for Great Britain — since the mid-19<sup>th</sup>  
112 Century. Despite representing a potentially valuable source for deriving long-term change in land

113 use or land cover, studies assessing the use of such information are scarce (e.g. Hooftman &  
114 Bullock, 2012).

115         The aim of this study is to utilise historical topographic maps for semi-automated  
116 mapping of urban land use change and change in impervious cover. Two novel methods are  
117 presented that utilise topographic maps to: i) derive maps of fractional impervious surface for  
118 direct computation of catchment-level imperviousness; ii) derive maps of urban land use for  
119 subsequent computation of estimates of catchment-level imperviousness based on an urban  
120 extent index. Impervious surface cover estimates computed using these two methods are  
121 validated using reference data generated through a RS-based image classification of high-  
122 resolution aerial photographs. The methods presented herein are employed in an attempt to  
123 determine their suitability for indicating change in urban land use and imperviousness — here  
124 throughout a 50-year period from 1960–2010 in a number of hydrological catchments  
125 surrounding a UK town that exemplifies rapid peri-urban development.

126

## 127 **2. Study area**

128         The study area (Fig. 1) encompasses two adjacent small urban stream catchments located  
129 to the north of Swindon in the south of England; comprising the Haydon Wick brook and  
130 Rodbourne stream, both tributaries of the River Thames (Fig. 1 inset). Swindon was designated  
131 as an Expanded Town under the Town Development Act in 1952 which encouraged town  
132 development in county districts to relieve over-population elsewhere. The Rodbourne stream  
133 catchment has been highly urbanised since the 1950s and comprises a large area of commerce  
134 and industry on the northern edge of Swindon town, along with highly urbanised housing  
135 developments. The Haydon Wick brook catchment is located further to the north of Swindon and

136 has undergone widespread development since the 1990s, prior to which it was a predominantly  
137 agricultural landscape. Within the Haydon Wick catchment a number of distinct catchments (1-  
138 5) have been selected (Fig. 1) that capture and reflect the diversity and age of different  
139 developments within the area. The Rodbourne catchment, in which development has  
140 incrementally expanded since the 1950s, remains one single catchment unit (6) for this study.  
141 The focus of this study is to test two methodologies for mapping changes in urban land use and  
142 associated imperviousness in each of these six catchments during the period 1960 to 2010.

143 **INSERT FIG.1 HERE**

144

### 145 **3. Material and methods**

146 The ability to utilise traditional topographic maps for long-term, historical mapping of urban  
147 extent and estimation of catchment imperviousness is assessed using a three-pronged approach  
148 (Fig. 2). The approach involves first estimating contemporary catchment fractional impervious  
149 surface area directly from aerial photographs for use as reference data. These reference data are  
150 then used to validate the two methods presented in this paper for mapping historical change in  
151 impervious cover topographic maps. Following validation, a comparison of the two methods is  
152 undertaken to assess their relative performance revealing long-term change in catchment  
153 impervious cover between 1960 and 2010. More detailed information regarding the  
154 methodological approach is provided in the following sub-sections.

155 **INSERT FIG. 2 HERE**

#### 156 ***3.1 Deriving catchment imperviousness from aerial photographs***

157 Reference data for quantifying the catchment fractional impervious cover were obtained  
158 from aerial photographs for three decadal time-slices within the 50-year period of interest —  
159 namely 1991, 1999 and 2010 (herein referred to as 1990, 2000 and 2010, respectively). The  
160 reference data were generated by first classifying 0.5 m true-colour aerial photographs into  
161 pervious land cover classes: grass, trees, bare soil and water; and impervious land cover classes:  
162 roads/pavements, commercial buildings and residential buildings. It was anticipated that land  
163 cover classes such as bare soil and roofing tiles could be particularly difficult to discriminate  
164 using the limited spectral information contained in only the red, green, blue bands of the aerial  
165 photographs. Therefore, textural information was also incorporated in the form of the Grey-Level  
166 Co-occurrence Matrix (GLCM) parameters of entropy, dissimilarity, second moment and  
167 homogeneity (Haralik et al. 1973; Herold et al., 2003). These parameters were derived from the  
168 green band in the ENVI 4.8 software package (Research Systems, Inc.) for a  $3 \times 3$  pixel (i.e. 1.5  
169 m  $\times$  1.5 m) window and a co-occurrence window shift of 4 pixels (i.e., 2 m) in both the x- and y-  
170 direction. This combination of window size and shift was chosen as it maximised visual  
171 discrimination of the different land cover classes.

172 Classification of the three time-slices employed a neural network (NN) classification  
173 algorithm in conjunction with the seven associated spectral and textural bands. A NN classifier  
174 was chosen because they are capable of producing better classification results for complex  
175 heterogeneous urban areas than their conventional counterparts (e.g., Maximum Likelihood),  
176 since they are non-parametric and more robust in handling noisy and non-normally distributed  
177 data (Foody, 2002; Lu & Weng, 2009). The NN used in this case was a Multi-Layered  
178 Perceptron NN with a back-propagation learning algorithm for supervised learning (Richards &  
179 Jia, 2006). Using a three-layered NN (i.e., input, output and one hidden layer), land cover

180 classifications were performed in ENVI 4.8 with the default training parameters confirmed  
181 through a set of trial-and-error experiments. Each classification was supervised with the aid of a  
182 set of training pixels that were carefully selected in the imagery to represent each of the defined  
183 land cover types (~6000 pixels for each class).

184 Land cover classifications were converted to binary imperviousness maps by collapsing  
185 the classes into just two corresponding to pervious or impervious surfaces (Yuan & Bauer, 2006;  
186 Im et al., 2012; Amirsalari et al., 2013). The accuracies of the resulting binary imperviousness  
187 maps were determined by comparing the true class identities of a sample of validation pixels to  
188 the classes assigned through classification. Validation pixels were selected from regions of  
189 interest (ROIs) of known pervious or impervious surface class identities that were defined in  
190 each time-slice image based on extensive knowledge of the study area. Validation pixels were  
191 then selected from the ROIs using a random stratified sampling protocol to ensure each class was  
192 represented proportionately, and to avoid spatial autocorrelation within the validation dataset  
193 (Chini et al., 2008; Pacifici et al., 2009). The minimum validation sample size required to derive  
194 statistically valid accuracy estimates for the entirety of each binary map was determined from the  
195 normal approximation of the binomial distribution (Fitzpatrick-Lins, 1981). Consequently —  
196 based on an expected accuracy of 50% and a precision of  $\pm 0.5\%$  at the 95% confidence level —  
197 approximately 19,000 validation pixels for each class were selected to determine the accuracy of  
198 each binary imperviousness map.

199 Binary imperviousness map accuracies were assessed by way of the overall (OA), user's  
200 (UA) and producer's (PA) accuracies and the Kappa coefficient (K) derived from a confusion  
201 matrix (Congalton, 1991). The overall accuracy is the percentage of all validation pixels  
202 correctly classified, whereas the user's and producer's accuracies provide information regarding

203 the commission and omission errors associated with the individual classes, respectively.  
 204 Following validation, the 0.5 m binary impervious maps were aggregated to 50 m grid cells to  
 205 generate fractional impervious surface maps, with the value for each grid cell corresponding to  
 206 the proportion of impervious pixels within it. The value of 50 m was selected as it was found to  
 207 best represent homogeneous scale of urban land use classification (see 3.2.2). The  
 208 imperviousness of each of the six catchments ( $\%IMP$ ) was then computed from these fractional  
 209 impervious surface maps for use as reference data, using:

$$210 \quad \%IMP = \frac{\sum_i^n (\%IMP_i \times A_i)}{A_c}, \quad (1)$$

211 where  $\%IMP_i$  is the fractional impervious cover for grid cell  $i$ ,  $A_i$  is the area of the grid cell,  $n$  is  
 212 the number of grid cells within the catchment, and  $A_c$  is the total catchment area.

213

### 214 ***3.2 Deriving estimates of catchment imperviousness using topographic maps***

215 As outlined in Fig. 2, estimates of catchment fractional impervious surface cover were  
 216 derived using two methods. In general, these consist of first generating binary imperviousness  
 217 maps from the topographic maps and then computing catchment imperviousness from either  
 218 fractional imperviousness maps or urban land use maps — as illustrated in Fig. 3 and described  
 219 below.

220

#### 221 **3.2.1 Data and pre-processing**

222 Digital historical topographic maps produced by the UK Ordnance Survey (OS) between  
 223 1960 and 2010 were obtained in raster format as 25 km x 25 km tiles with a 1 m spatial  
 224 resolution. For each decade (1960s to 2010s), the most contemporaneous map tiles produced for

225 that decadal time-slice were obtained and mosaicked to produce a seamless image for each  
226 decade (Table 1). The primary step for the two methods is to convert the historical topographic  
227 maps into simplified and physically representative binary maps of developed (i.e., impervious)  
228 and undeveloped (i.e., pervious) pixels. To do this, the original pixel values were reclassified so  
229 that a value of 1 was assigned to pixels corresponding to ‘white space’ on the map and a value of  
230 2 to all pixels corresponding to mapped features.

231 **INSERT FIG 3. HERE**

232 **INSERT TABLE 1 HERE**

233 Due to slight variations in the cartographic style used from 1960 to 2010, a number of  
234 steps were required to further improve the consistency and compatibility of each map. The first  
235 stage involves developing ‘level-1’ binary maps, in which artefacts and key inconsistencies  
236 between maps from each decade are reduced. This was undertaken using the ‘Raster Cleanup’  
237 tool in ArcMap (ArcGIS 10, ESRI) and included the following steps:

- 238 • A rapid ‘clean-up’ of each raster map is undertaken to remove features, such as place  
239 names or symbols relating to wide-spread forest;
- 240 • Reclassifying large concrete or tarmac areas represented by ‘white space’ to developed  
241 areas;
- 242 • Infilling the roofs of large buildings on raster maps for 2000–2010 due to the low density  
243 of pixels used to represent such areas on these maps.

244 A second pre-processing stage was subsequently applied for the purpose of infilling  
245 developed features such roads and buildings to generate a set of ‘level-2’ binary maps. This was  
246 undertaken in ArcMap by applying the ‘Boundary Clean’ tool to each raster and then converting  
247 them to polygon shapefiles. This conversion enables road segments and buildings to be readily

248 reattributed to alter them from polygons representing pervious (undeveloped) features to  
249 impervious (developed) features. Once all relevant polygons have been reassigned, the shapefiles  
250 were then converted back to raster format.

251

### 252 **3.2.2 Deriving catchment imperviousness from fractional impervious surface maps**

253 The first method (method 1) for deriving catchment imperviousness for the six  
254 catchments is relatively straightforward to implement, and is focussed on the generation of  
255 fractional impervious surface maps of the study area. To generate these maps, the ‘level-2’  
256 binary maps derived from the topographic maps were aggregated to 50 m grid cells in a similar  
257 manner to that used to derive fractional impervious surface maps from the aerial photographs. In  
258 this case, the value for each 50 m grid cell is calculated as the proportion of 1 m impervious  
259 pixels contained within it. Although pre-processing steps were implemented to improve the  
260 compatibility and consistency of the topographic map time series (1960–2010), additional  
261 calibration was performed to account for any residual discrepancies between the fractional  
262 impervious surface maps. Adopting the approach outlined by Lu et al. (2011), pseudo-invariant  
263 pixels (i.e., those remained unchanged in terms of imperviousness throughout the time series)  
264 were selected for pair-wise image calibration via linear regression models. As a result, all  
265 fractional impervious surface maps were calibrated to the most recent map (i.e., 2010). Once  
266 calibrated, the imperviousness of each of the six catchments ( $OS_{\%IMP}$ ) is computed from these  
267 calibrated fractional impervious surface maps using an adaptation of Eq. 1, and compared with  
268 the contemporaneous reference data derived from aerial photography ( $\%IMP$ ).

269

270

271

272 **3.2.3 Deriving catchment impervious cover from urban land use maps**

273 The second method (method 2) for deriving catchment imperviousness for the six  
274 catchments is based on the generation of urban land use maps from the topographic maps. Maps  
275 of urban land use were generated by aggregating the topographic map-derived binary maps for  
276 each decade to larger grid cells, and then classifying the cells according to the LCM land  
277 use/land cover definitions; mixed development and green space designated as Suburban (e.g.,  
278 houses with gardens), areas of near continuous development with little vegetation (e.g., industrial  
279 estates) designated continuous Urban (Fuller et al., 2002), and all other areas of green and  
280 general pervious surfaces referred to as Rural. Following a preliminary evaluation of a number of  
281 different grid cell sizes, a cell size of 50 m was identified as the optimum for generating realistic,  
282 homogeneous urban land use maps; smaller cell sizes produced maps with the aforementioned  
283 ‘speckled’ effect that often affects per-pixel classification in urban areas. Additionally, it was  
284 found that application of this approach to the ‘level-2’ binary grids resulted in difficulty devising  
285 a standard classification which can be used to produce coherent land use maps across the time  
286 series. For this reason, the ‘level-1’ binary maps derived from the topographic maps were used to  
287 generate the land use maps. This was achieved using ArcMap through the following steps:

- 288 • ‘Level-1’ binary maps were aggregated using the ‘Aggregate’ function to generate a  
289 grid that details the mean value of the pixels contained within each 50 m grid cell.  
290 These aggregated values provide an indication of the level of development; 50 m grid  
291 cells with a value close to 1 essentially correspond to ‘white space’ (i.e., a rural  
292 undeveloped area), whereas a value close to 2 corresponds to a high density of  
293 mapped features (i.e., a highly developed area).

294           • A threshold-based classification scheme was then applied to the grid in order to  
295           assign cells to either the Urban, Suburban or Rural land use class. It was found that  
296           cell values of 1–1.35 represented Rural land use, values of 1.35–1.65 corresponded to  
297           Suburban, and values above 1.65 represented Urban land use. These thresholds were  
298           validated to ensure at least 80% of 50 randomly selected grid cells were correctly  
299           classified in decadal map. The output is set of 50 m maps showing Rural, Suburban,  
300           and Urban land use (shown in Fig. 3).

301           Potentially erroneous pixel classifications were removed through geo-spatial proximity  
302           analysis, and by applying an urban land use change trajectory demonstrated by Verbeiren et al.  
303           (2013) to ensure greater consistency throughout the time series. This is achieved by first  
304           combining the ArcGIS ‘Conditional’ tool in the ‘Raster Calculator’ with the ‘Focal Statistics’  
305           tool to identify misclassified Urban and Suburban grid cells based on the classes of neighbouring  
306           cells — isolated Suburban or Urban cells were reclassified according to the dominant  
307           surrounding class. Following this, each cell was labelled as either 0 (Rural), 1 (Suburban) or 3  
308           (Urban) and all trajectories of land use change were recorded throughout the time series using  
309           codes (e.g., 00112, 01222, etc). These were then evaluated according to whether they reflect  
310           realistic changes observed in the catchment over the study period, and subsequently classified  
311           into 6 rationality classes: ‘urban growth’, ‘suburban growth’, ‘urban regeneration’, ‘urban  
312           stability’, ‘suburban stability’, and ‘inconsistent’. The ‘inconsistent’ class captures grid cells that  
313           do not follow realistic change trajectories — such as a Suburban area changing to Rural then  
314           Suburban and back to Rural. Inconsistent cells were corrected using the most likely trajectory for  
315           that cell over the 50 year period – based upon surrounding cells. The class ‘urban regeneration’  
316           captures the possibility of Urban areas being demolished and replaced with green space or

317 subsequent re-development. The land use change trajectory rules were implemented using the  
318 ‘Conditional’ tool in the ArcMap ‘Raster Calculator’. The outcome was as set of coherent urban  
319 land use maps revealing the long-term change in land use for the period 1960–2010.

320 For each land use map, the proportions of Urban and Suburban grid cells within each  
321 catchment were used to calculate a catchment index of urban extent. As well as measuring the  
322 urban extent within a hydrological catchment, the index of urban extent (*URBEXT*) proposed in  
323 the UK Flood Estimation Handbook (FEH) methodology (Institute of Hydrology, 1999) can also  
324 provide an estimate of the impervious surface cover. Accordingly, the index of urban extent and  
325 estimate of imperviousness for the six catchments (*URBEXT*) in each land use map is computed  
326 using:

$$327 \quad \textit{URBEXT} = \textit{Urban} + (\beta \times \textit{Suburban}), \quad (2)$$

328 where *Urban* and *Suburban* are the proportions of Urban and Suburban grid cells within each  
329 catchment, respectively, and  $\beta$  is the Suburban weighting factor. The suitability of *URBEXT* for  
330 estimating catchment imperviousness is assessed through comparison with the reference data  
331 derived from aerial photography (*%IMP*). For the purpose of this comparison, *URBEXT* — the  
332 weighted value of urban extent within a catchment — is considered to provide a direct estimate  
333 of the catchment percentage imperviousness. The Suburban weighting factor ( $\beta$ ) is preset to a  
334 value of 0.5 to account for the general equal mixture of built-up land and permanent vegetation  
335 (Institute of Hydrology, 1999). Urban land use was assigned a weighting of 1 because such areas  
336 generally have negligible green (pervious) space. In an attempt to improve the accuracy of the  
337 catchment imperviousness estimates, an optimal value for  $\beta$  was sought by applying a linear  
338 regression model between reference imperviousness (*%IMP*) and *URBEXT* across the three

339 decadal time-slices. This provides a refined calibrated value of catchment impervious surface  
340 ( $URBEXT_{IMP}$ ).

341

## 342 **4. Results and discussion**

### 343 ***4.1 Imperviousness maps from aerial photography***

344 The accuracies of the RS-derived high-resolution (0.5 m) maps of binary imperviousness  
345 for 1990, 2000 and 2010 are shown in Fig. 4. High overall accuracies ( $> 86\%$ ) were achieved in  
346 all three cases and are also confirmed by the corresponding K values (0.74–0.83); interpreted as  
347 reflecting a “substantial” to “almost perfect” degree of accuracy (Landis & Koch, 1977). Further  
348 corroboration of the classification accuracy is provided by the high user’s (88–99%) and  
349 producer’s (77–89%) accuracies associated with both the pervious and impervious classes in all  
350 binary imperviousness maps; indicating low commission and omission errors, respectively. The  
351 result of this accuracy assessment indicate that the binary imperviousness maps are suitable for  
352 deriving reference data for validating the estimates of catchment imperviousness computed using  
353 the topographic map-based methods.

354 **INSERT FIG. 4 HERE**

355

### 356 ***4.2 Catchment imperviousness from fractional impervious surface maps***

357 Catchment imperviousness obtained from topographic map-derived fractional impervious  
358 surface maps ( $OS_{\%IMP}$ ) — method 1 — was compared with the reference data ( $\%IMP$ ) derived  
359 from the aerial photographs (Fig. 5). A reasonable, but variable level of agreement between  
360  $OS_{\%IMP}$  and  $\%IMP$  is observed throughout the three decadal time-slices. Although the correlation  
361 for 1990 is greatest ( $R^2 = 0.96$ ), the catchment imperviousness measured using  $OS_{\%IMP}$  is  
362 consistently (with the exception of catchment 3) approximately 10% larger than the reference

363 data. The general overestimation of  $OS_{\%IMP}$  is most likely attributable to the larger size  
364 depictions of features such as roads on the 1990 topographic map, compared to equivalent  
365 features on the more recent maps. The correlation between  $OS_{\%IMP}$  and  $\%IMP$  is somewhat  
366 lower for both 2000 and 2010 ( $R^2 = 0.75$  and  $0.62$ , respectively), with the data appearing more  
367 widely distributed around the reference  $\%IMP$ . This observed decrease in the level of agreement  
368 could be due a slight offset in the exact instant in time at which the aerial photographs and  
369 corresponding topographic maps capture. Alternatively, this could arise due to the slightly lower  
370 accuracies of the 2000 and 2010 aerial photography-derived binary imperviousness maps, in  
371 comparison to the 1990 map. Nevertheless, the results suggest that estimating catchment  
372 imperviousness using fractional impervious surface maps derived from topographic maps (i.e.,  
373 method 1) is feasible.

374 **INSERT FIG. 5 HERE**

375

### 376 ***4.3 Mapping urban land use change using topographic maps***

377 Urban land use derived from the topographic maps using method 2 reveals the spatio-  
378 temporal change in Urban, Suburban and Rural land use at a decadal intervals from the 1960s to  
379 2010s (Fig. 6). While the highly urban Rodbourne catchment (catchment 6) exhibits a gradual  
380 expansion and infilling of Urban and Suburban land use, the Haydon Wick catchments (1–5)  
381 exhibit a more dramatic and rapid changes in land use over the 50-year study period. The  
382 remarkable change from predominantly Rural (agricultural) land use in all Haydon Wick  
383 catchments (1–5) to predominantly Suburban land use is clearly illustrated in Fig. 7, as is the  
384 impact of one large commercial development in catchment 2 in the 2000's. The relative change  
385 that occurred in catchment 6, which was already over 50% Suburban in 1960, is significantly less

386 than in the peri-urban area of the Haydon Wick catchments (Fig. 7). In all cases, the mapped  
387 spatio-temporal changes in Urban land use were found to be consistent with the physical changes  
388 observed in the original OS topographic maps. By the 2010s, the relative proportion of  
389 developed (i.e., Urban or Suburban) land across all catchments is high and the remaining Rural  
390 areas typically represent areas of green space designated for recreation and conservation, along  
391 with areas of significant flood risk.

392 **INSERT FIG. 6 HERE**

393 **INSERT FIG. 7 HERE**

394 **INSERT TABLE 2 HERE**

395 Catchment values of *URBEXT* computed using the land use maps (Table 2) also show  
396 distinct differences between the Haydon Wick catchments (1–5) and Rodbourne catchment (6).  
397 During the period 1960–2010, *URBEXT* values changed little across the Rodbourne catchment,  
398 with only a 14.2% increase as a result of small, steady incremental change during each decade.  
399 More significant change across the Haydon Wick catchments reflects successive waves of peri-  
400 urban development during the study period, with an average overall increase in *URBEXT* of  
401 35.4% and significant variation between the catchments (17.5–41.3%). Again, the observed  
402 temporal changes in urban extent were found to be consistent with known physical changes that  
403 occurred within the period 1960–2010. Therefore, the results demonstrate that the employed  
404 method is an effective approach for readily mapping long-term basic land use change and  
405 associated catchment-level urban extent from historical topographic maps. A particular important  
406 stage in this methodology is the application of land use trajectory analysis (e.g., Verbeiren et al.,  
407 2013), which was crucial in ensuring a reliable time series dataset from which only genuine land  
408 use change is revealed.

409

410 **4.4 Catchment imperviousness from urban land use maps**

411 To investigate whether a simple index of urban extent (*URBEXT*) derived from  
412 topographic maps can provide representative estimates of catchment imperviousness, a  
413 comparison with reference imperviousness derived from aerial photography (*%IMP*) was  
414 undertaken (Fig. 8). Overall, a high correlation between *URBEXT* and *%IMP* is observed across  
415 most catchments during the three decades ( $R^2 = 0.80\text{--}0.96$ ), and also when all data is considered  
416 collectively ( $R^2 = 0.86$ ). Nevertheless, some notable deviations were observed for specific  
417 catchments and time-slices. For example, values of *%IMP* for catchment 3 were shown to be  
418 much higher than *URBEXT* in all cases due to significant underestimation of Urban areas of  
419 gravel and tarmac because of their depiction on topographic maps. Also, for 1990, *URBEXT*  
420 values are clustered around *%IMP*, while *URBEXT* consistently underestimates catchment  
421 imperviousness for both 2000 and 2010. The general underestimation of catchment  
422 imperviousness is likely to relate to the use of the ‘level-1’ binary grids, in which buildings and  
423 roads are not infilled. Nonetheless, it is apparent that land use maps generated from topographic  
424 maps can be used in conjunction with the urban index, *URBEXT*, (i.e., method 2) to generate  
425 feasible estimates of catchment imperviousness.

426 **INSERT FIG. 8 HERE**

427 A linear regression model between *URBEXT* and *%IMP* across the three decadal time-  
428 slices returned an optimised Suburban weighting factor ( $\beta = 0.53$ ). Calibrated values of urban  
429 extent (*URBEXT<sub>IMP</sub>*) for each catchment were computed for 1990, 2000 and 2010 by using this  
430 optimised value for  $\beta$  in Eq. 2. Following a comparison, the overall correlation between  
431 *URBEXT<sub>IMP</sub>* and *%IMP* ( $R^2 = 0.84$ ) was actual found to be marginally lower than for *URBEXT*  
432 ( $R^2 = 0.86$ ), indicating that the original preset  $\beta$  (0.5) was more appropriate in this particular case.

433 However, in regions where Suburban land use does not comprise equal mixtures of built-up land  
434 and vegetation, the optimal weighting can be determined using the same approach as that used  
435 here. Given its slightly better performance with respect to %IMP, estimates of catchment  
436 imperviousness computed using *URBEXT* are used for subsequent analysis.

437

#### 438 ***4.5 Historical change in imperviousness***

439 The two methods employed for computing catchment imperviousness from topographic  
440 maps in this study both provide a means of revealing long-term change in imperviousness. As  
441 illustrated by Fig. 9, the overall trend in imperviousness change for 1960–2010 is consistent  
442 between the two methods. With the exception of catchment 6, which was already highly  
443 developed prior to 1960, all catchments experience a somewhat rapid increase in imperviousness  
444 during a specific period between 1960 and 2010. For example, catchment 1 sees its biggest  
445 increase in imperviousness during 1980–1990, while catchment 3 experiences a rapid rise during  
446 1990–2000. The timings of these rapid increases in imperviousness coincide with known  
447 episodes of peri-urban expansion within the study area, and reflect the pattern of continuous  
448 growth and expansion where when one development finishes just shortly before another one  
449 commences. The less dramatic change observed for catchment 5 can be explained by the fact that  
450 it already contained suburban housing stock in 1960 and that it also contains a large nature  
451 reserve which is protected from development.

#### 452 **INSERT FIG. 9 HERE**

453 In addition to displaying similar trends, the two methods provide very similar estimates  
454 of the total absolute change in catchment imperviousness between 1960 and 2010. The mean  
455 difference in the total absolute change estimates between the two methods, for all catchments, is  
456 2.9%, with individual catchment estimates varying between a maximum difference of 7.1% and a

457 minimum of 0.4%. The maximum difference is associated with catchment 6, which is arguably  
458 the most complex in terms of land use change during 1960–2010 because of gradual expansion  
459 of the industrial area in the south-eastern section of the catchment, and regeneration of the  
460 railway network to suburban housing in the south-west. As illustrated by Fig. 9, the more rural  
461 northern catchments (i.e., 1–4) experienced the most significant total absolute change in  
462 catchment impervious across the entire study period, with increases of between 36% and 42%.  
463 These estimates clearly reflect the rapid expansion of suburban land use into these previously  
464 rural areas as revealed in Fig. 6.

465         Although Fig. 9 illustrates that the methods reveal similar trends and estimates of change  
466 in imperviousness across the six catchments for 1960–2010, there are differences in the  
467 individual catchment imperviousness estimates. Specifically, all estimates computed using  
468 method 1 (*OS<sub>%IMP</sub>*) exceed those produced using method 2 (*URBEXT*), with a mean absolute  
469 difference of 7.8% (Table 3). With respect to the time intervals, the largest differences between  
470 the methods occurs for the years 1990 and 2000, where *OS<sub>%IMP</sub>* estimates are respectively 8.3%  
471 and 9.4% greater than the equivalent *URBEXT* estimates. With respect to catchments, the largest  
472 differences between methods are observed for catchments 5 and 6, for which *OS<sub>%IMP</sub>* estimates  
473 are respectively 9.0% and 9.5% greater than *URBEXT* estimates. The overall trend of method 1  
474 producing higher estimates than method 2 is explained by a combination of the contrasting  
475 representation of features such as roads and buildings in the different binary maps (i.e., the level  
476 of infilling) incorporated in the two methods, and the somewhat simplistic discrete weighting  
477 system employed in method 2. In particular, the infilling of features such as roads in the level 1  
478 binary maps used in method 1 can lead to overestimation of impervious cover as the symbology  
479 used represent roads does not always reflect the true physical dimensions, and can lead to infill

480 of isolated areas that are not physically developed. Despite the fundamental differences in the  
481 two methods, both have been demonstrated to be feasible approaches for computing catchment  
482 imperviousness and its historical change from topographic maps.

483 **INSERT TABLE 3 HERE**

484

#### 485 **4.6 Considerations in using topographic maps for estimating imperviousness**

486 This paper demonstrates, through two methods, that topographic maps can be used to  
487 compute estimates of catchment imperviousness. When contemplating the use, or evaluating the  
488 performance, of *OS%IMP* and *URBEXT* — or any other topographic map-based method — there  
489 are a several aspects that require some consideration:

- 490 I. Aerial photographs and topographic maps do not necessarily represent the exact same  
491 instant in time, since whereas aerial photographs provide a snapshot for a specific  
492 date, topographic maps incorporate updates within a given time period (see Table 1).
- 493 II. Failure to remove place names and symbols (e.g., to represent forests) from the  
494 topographic maps will translate to the subsequently derived binary maps and lead to a  
495 degree of overestimation of imperviousness – users should ensure some consistent  
496 criteria are outlined for any manual interventions.
- 497 III. Topographic maps do not readily discriminate areas of inland bare ground and  
498 concrete/tarmac features, which will subsequently lead to their misrepresentation on  
499 derived binary impervious surface maps and result in a degree of underestimation of  
500 imperviousness. However, infilling of features such as roads can lead to  
501 overestimation of impervious cover if the symbology used does not directly reflect  
502 true physical dimensions.

503 IV. Small-scale features (e.g., minor roads) and minor changes within existing  
504 development boundaries (e.g., infilling or ‘urban creep’) shown on aerial photography  
505 are not always captured using the discrete land use classification and scale employed  
506 in method 2.

507 V. Calibration of the fractional impervious surface maps (as in method 1) and  
508 implementation of land use trajectory analysis (method 2) are crucial steps in  
509 producing a coherent time series dataset for revealing reliable long-term change in  
510 imperviousness.

511 With both methods capable of providing good estimates of catchment imperviousness,  
512 the most appropriate method is largely dependent on the purpose of the study and the format of  
513 the topographic maps. In general, method 1 can be more readily implemented and provides maps  
514 of fractional impervious surfaces, thus describing imperviousness on a continuous scale (Fig.  
515 10). On the other hand, despite method 2 providing only a discrete description of imperviousness  
516 (see Fig. 10), it does provide maps of general land use that are informative when interpreting  
517 changes in imperviousness over time. Although method 1 can be readily applied to any study  
518 area, as demonstrated here, method 2 can be calibrated to determine the optimal weighting factor  
519 associated with Suburban land use ( $\beta$ ). Additionally, if the available topographic maps depict  
520 roads and building as infilled features (akin to the ‘level-2’ binary maps) then method 1 would be  
521 more suitable. However, if — as in the case of the OS topographic maps used here — such  
522 features are not infilled, then method 2 can be applied without the need of additional pre-  
523 processing steps to produce ‘level-2’ binary maps.

524 **INSERT FIG. 10 HERE**

525

## 526 **6. Conclusions**

527         This paper demonstrates that it is possible to derive robust long-term estimates of  
528 catchment imperviousness from topographic maps using two different contrasting methods. The  
529 first method (method 1) generates fractional impervious surface maps from the topographic maps  
530 and uses these to estimate catchment imperviousness. The second method (method 2) generates  
531 generalised land-use maps from the topographic maps and then computes catchment  
532 imperviousness from these using an index of urban extent. Although some degree of manual  
533 intervention is required for both methods, the processing stages employed are largely semi-  
534 automatic and require significantly less time than manual delineation of impervious surfaces.  
535 Such manual intervention will rely on some degree of user subjectivity – related to the format of  
536 the topographic maps – that could alter the binary maps and derived impervious cover products.  
537 Such interventions are required to produce more consistent mapping products for derivation of  
538 binary maps, and it is recommended that users employ transparency in the reporting of such  
539 interventions. Through comparison with reference data obtained using aerial photographs, it is  
540 demonstrated that both methods are capable of providing accurate estimates of catchment  
541 imperviousness and its change over time. With both methods capable of providing good  
542 estimates of catchment imperviousness, the most appropriate method beyond this study will be  
543 largely dependent on the purpose of the study and the format of the topographic maps.

544         This study demonstrates that both methods show the peri-urban Haydon Wick catchment  
545 has undergone a significant change from predominantly rural to highly urban and is now  
546 dominated by suburban areas of housing development. Findings from hydrological studies (e.g.  
547 Braud et al., 2012; Dams et al., 2012) would suggest that this will have led to a faster catchment  
548 response and greater magnitude of flow during storm events – making the area more prone to

549 flooding. Local reports of more frequent flooding would be consistent with this hypothesis but  
550 hydrological modelling of the change in storm runoff response would be necessary to validate  
551 this assumption.

552         Several issues that may affect derived estimates of catchment imperviousness using  
553 topographic maps are highlighted for consideration in future applications of this methodology.  
554 For example, catchments containing large areas of concrete, gravel and tarmac (e.g., car parks)  
555 might not be recognisable as developed surfaces on topographic maps. Conversely, although  
556 such surfaces are typically characterised as impervious, they are not always physically  
557 impervious *per se*. For example, gravel cover is not inherently impervious and more modern car  
558 parks and roads can employ Sustainable Urban Drainage Systems (SUDS) design principles to  
559 enable infiltration of water to the media below. Furthermore, the presence and spatial distribution  
560 of both traditional drainage systems and SUDS contribute to the effective impervious area (EIA)  
561 — the connectivity to impervious areas — and are shown to be a strong determinant of storm  
562 runoff response (Han & Burian, 2009). This highlights the limitation of using simple impervious  
563 area estimates in hydrological studies. Also, depending on the maps scale, plot-scale (changes  
564 such as housing extensions driving urban creep; Perry & Nawaz, 2008) may not be captured on  
565 topographic maps.

566         Further research is required to progress to a more realistic scheme which accounts for  
567 varying degrees of imperviousness within individual land use or land cover classes. This would  
568 require better characterisation of urban typologies and land cover classes in terms of their natural  
569 permeability, association with drainage systems, and additional factors which affect the  
570 catchment runoff response. Such information would have to be obtained from auxiliary datasets  
571 as this is not readily available on historical topographic maps. Imperviousness maps

572 incorporating information on connectivity and features that influence hydrological response to  
573 storm events would be particularly useful in quantifying the impact of historical urbanisation on  
574 flooding.

575

## 576 **Acknowledgements**

577 The authors would like to thanks Thomas Kjeldsen and France Gerard of the Centre for Ecology  
578 and Hydrology and Rachel Dearden of the British Geological Survey for their contributions. We  
579 are also thankful to the two anonymous reviewers for their comments and suggestions, which  
580 helped to improve the quality of this manuscript.

581

## 582 **References**

583 Amirsalari, F., Li, J., Guan, X., & Booty, W. G. (2013). Investigation of correlation between  
584 remotely sensed impervious surfaces and chloride concentrations. *International Journal*  
585 *of Remote Sensing*, 34, 1507–1525.

586 Arnold, C. L., & Gibbons, C. J. (1996). Impervious Surface Coverage: The emergence of a key  
587 environmental indicator. *Journal of the American Planning Association*, 62, 243–258.

588 Banzhaf , E., Grescho, V., & Kindler, A. (2009) .Monitoring urban to peri-urban development  
589 with integrated remote sensing and GIS information: a Leipzig, Germany case study,  
590 *International Journal of Remote Sensing*, 30, 1675–1696.

591 Barredo, J. I., Kasanko, M., McCormick, N., & Lavalle, C. (2003). Modelling dynamic spatial  
592 processes: simulation of urban future scenarios through cellular automata. *Landscape and*  
593 *Urban Planning*, 64, 145–160.

594 Bauer, M. E., Heinert, N. J., Doyle, J. K., & Yuan, F. (2004). Impervious surface mapping and

- 595 change monitoring using Landsat remote sensing. *ASPRS Annual Conference*  
596 *Proceedings, Denver, Colorado, May 2004.*
- 597 Bayliss, A. C., Black, K. B., Fava-Verde, A., & Kjeldsen, T. R. (2006). URBEXT<sub>2000</sub> – A new  
598 FEH catchment descriptor: Calculation, dissemination and application. *Joint Defra/EA*  
599 *Flood and Coastal Erosion Risk management R & D Programme. R&D Technical Report*  
600 *FD 1919/TR*, (pp. 49).
- 601 Benz, U. C., Hofmann, P., Willhauck, G., Lingenfelder, I., & Heynen, M. (2004). Multi-  
602 resolution, object-oriented fuzzy analysis of remote sensing data for GIS-ready  
603 information. *ISPRS Journal of Photogrammetry and Remote Sensing*, 58, 239–258.
- 604 Bibby, P. (2009). Land use change in Britain. *Land Use Policy*, 26, S2–S13.
- 605 Braud, I., Breil, P., Thollet, F., Lagouy, M., Branger, F., Jacqueminet, C., Kermadi S, & Michel  
606 K. (2012). Evidence of the impact of urbanization on the hydrological regime of a  
607 medium-sized periurban catchment in France. *Journal of Hydrology*, 485, 5–23.
- 608 Chini, M., Pacifici, F., Emery, W. J., Pierdicca, N., & Del Frate, F. (2008). Comparing statistical  
609 and neural network methods applied to very high resolution satellite images showing  
610 changes in man-made structures at rocky flats. *IEEE Transactions on Geoscience and*  
611 *Remote Sensing*, 46, 1812–1821.
- 612 Congalton, R.G. (1991). A review of assessing the accuracy of classifications of remotely sensed  
613 data. *Remote Sensing of Environment*, 37, 35–46.
- 614 Dams, J., Dujardin, J., Reggers, R., Bashir, I., Canters, F., & Batelaan, O. (2013). Mapping  
615 impervious surface change from remote sensing for hydrological modelling. *Journal of*  
616 *Hydrology*, 485, 84–95.
- 617 Fitzpatrick-Lins, K. (1981). Comparison of sampling procedures and data analysis for a land-use and  
618 land-cover map. *Photogrammetric Engineering and Remote Sensing*, 47, 343–351.

- 619 Foody, G. M. (2002). Hard and soft classifications by a neural network with a non-exhaustively  
620 defined set of classes. *International Journal of Remote Sensing*, 23, 3853–3864.
- 621 Fuller, R. M., Smith, G. M., Sanderson, J. M., Hill, R. A., Thomson, A. G., Cox, R., Brown, N.  
622 J., Clarke, R. T., Rothery, P., & Gerard, F. (2002). Land Cover Map 2000: A Guide to the  
623 Classification System. *Countryside Survey 2000 Module 7, Final Report*.
- 624 Gerard, F., et al. (2010). Land cover change in Europe between 1950 and 2000 determined  
625 employing aerial photography. *Progress in Physical Geography*, 34, 183–205.
- 626 Han, W. S., & Burian, S. J. (2009). Determining effective impervious area for urban hydrologic  
627 modeling. *Journal of Hydrologic Engineering*, 14, 111–120.
- 628 Haralick, R. M., Shanmugan, K., & Dinstein, I. (1973). Textural features for image  
629 classification. *IEEE Transactions on Systems, Man, and Cybernetics*, 3, 610–621.
- 630 Herold, M., Liu, X., & Clarke, K. C. (2003). Spatial metrics and image texture for mapping  
631 urban land use. *Photogrammetric Engineering & Remote Sensing*, 69, 991–1001.
- 632 Hooftman, D. & Bullock, J. (2012). Mapping to inform conservation: A case study of changes in  
633 semi-natural habitats and their connectivity over 70 years. *Biological Conservation*, 145,  
634 30–38.
- 635 Hurd, J. D., & Civco, D. L. (2004). Temporal characterization of impervious surfaces for the  
636 State of Connecticut. *ASPRS Annual Conference Proceedings, Denver, Colorado, May*  
637 *2004*.
- 638 Im, J., Lu, Z., Rhee, J., & Quackenbush, L. J. (2012). Impervious surface quantification using a  
639 synthesis of artificial immune networks and decision/regression trees from multi-sensor  
640 data. *Remote Sensing of Environment*, 117, 102–113.

- 641 Institute of Hydrology. (1999). *Flood Estimation Handbook* (five volumes). Centre for Ecology  
642 and Hydrology, Oxfordshire, UK.
- 643 Kidd, C. H. R., & Lowing, M. J. (1979). The Wallingford urban subcatchment model. *Institute of*  
644 *Hydrology, Report No 60*. Wallingford, Oxfordshire, UK.
- 645 Kjeldsen, T. R. (2007). *The revitalised FSR/FEH rainfall-runoff method. Flood Estimation*  
646 *Handbook Supplementary Report No. 1*, Centre for Ecology & Hydrology, Wallingford,  
647 2007.
- 648 Kjeldsen, T. R., Svensson, C., Miller, J. M. (2012) Large-scale attribution of trend in UK flood  
649 flow data. In: *British Hydrological Society's Eleventh National Symposium, Dundee, 9–*  
650 *11 July 2012*. British Hydrological Society.
- 651 Landis, J. R., & Koch, G. G. (1977). The measurement of observer agreement for categorical  
652 data. *Biometrics*, 33, 159–174.
- 653 Lu D., Weng, Q., & Li, G. (2006). Residential population estimation using a remote sensing  
654 derived impervious surface approach. *International Journal of Remote Sensing*, 27,  
655 3553–3570.
- 656 Lu D., Moran, E., & Hetrick, S. (2011). Detection of impervious surface change with  
657 multitemporal Landsat images in an urban–rural frontier. *ISPRS Journal of*  
658 *Photogrammetry and Remote Sensing*, 66, 298–306.
- 659 Ogden, F. L., Pradhan, N. R., Downer, C. W., Zahner, J. A. (2011) Relative importance of  
660 impervious area, drainage density, width function, and subsurface storm drainage on  
661 flood runoff from an urbanized catchment. *Water Resources Research*, 47, W12503.

- 662 Pacifici, F., Chini, M., & Emery, W. J. (2009). A neural network approach using multi-scale  
663 textural metrics from very high-resolution panchromatic imagery for urban land-use  
664 classification. *Remote Sensing of Environment*, 113, 1276–1292.
- 665 Packman, J. (1980). The effects of urbanisation on flood magnitude and frequency. *Institute of*  
666 *Hydrology Report No 63*, Wallingford, Oxfordshire.
- 667 Perry, T., & Nawaz, R. (2008). An investigation into the extent and impacts of hard surfacing of  
668 domestic gardens in an area of Leeds, United Kingdom. *Landscape and Urban Planning*,  
669 86, 1–13.
- 670 Richards, J. A., & Jia, X. (2006). *Remote Sensing Digital Image Analysis, Fourth edition*. Berlin:  
671 Springer-Verlag, pp. 232–242.
- 672 Schueler, T. R. (1994). The Importance of Imperviousness. *Watershed Protection Techniques*, 1,  
673 100–111.
- 674 Shuster, W. D., Bonta, J., Thurston, H., Warnemuende, E., & Smith, D. R. (2005). Impact of  
675 impervious Surface on Watershed Hydrology. *Urban Water Journal*, 2, 263–75.
- 676 Tavares, A. O., Pato, R. L., & Magalhães, M. C. (2012). Spatial and temporal land use change  
677 and occupation over the last half century in a peri-urban area. *Applied Geography*, 34, 432–  
678 444.
- 679 Van de Voorde, T., De Genst, W., Canters, F., Stephenne, N., Wolff, E., & Binnard, M. (2003).  
680 Extraction of land use/land cover — Related information from very high resolution data  
681 in urban and suburban areas. *Proceedings of the 23rd Symposium of the European*  
682 *Association of Remote Sensing Laboratories* (pp. 237–244).

- 683 Van de Voorde, T., Jacquet, W., & Canters, F. (2011). Mapping form and function in urban  
684 areas: An approach based on urban metrics and continuous impervious surface data.  
685 *Landscape and Urban Planning, 102*, 143–155.
- 686 Vogel, R.M., Yaindl, C., & Walter, M. (2011). Nonstationarity: Flood Magnification and  
687 Recurrence Reduction Factors in the United States. *JAWRA Journal of the American*  
688 *Water Resources Association, 47*, 464–474.
- 689 Weng, Q. (2012). Remote sensing of impervious surfaces in the urban areas: Requirements,  
690 methods, and trends. *Remote Sensing of Environment, 117*, 34–49.
- 691 Yuan, F., & Bauer, M. E. (2006). Mapping impervious surface area using high resolution  
692 imagery: A comparison of object-based and per pixel classification. *American Society for*  
693 *Photogrammetry and Remote Sensing Annual Conference Proceedings, Reno, Nevada,*  
694 *2006.*
- 695 Zhou, Y. Y., & Wang, Y. Q. (2008). Extraction of impervious, surface areas from high spatial  
696 resolution imagery by multiple agent segmentation and classification. *Photogrammetric*  
697 *Engineering and Remote Sensing, 74*, 857–868.

698

## 699 **Figure captions**

700 Fig. 1. Map of the study area showing catchment boundaries and location of the study area  
701 within the Thames Basin (inset). RGB Aerial Photography – ©GeoPerspectives.

702 Fig. 2. Overview of methodological approach used to assess the utility of traditional topographic  
703 maps for long-term, historical mapping of urban extent and estimation of catchment  
704 imperviousness.

705 Fig. 3. Illustration of the approach applied in both method 1 and 2 to map impervious cover.  
706 cover (c) Crown copyright and Landmark Information Group.

707 Fig. 4. Classification accuracies of the binary imperviousness maps derived from aerial  
708 photographs for 1990, 2000 and 2010. OA — Overall accuracy; K — Kappa coefficient.

709 Fig. 5. Comparison of catchment imperviousness estimated from aerial photography ( $\%IMP$ ) and  
710 topographic map-derived fractional impervious surface cover ( $OS_{\%IMP}$ ) within the six  
711 catchments, for years 1990, 2000 and 2010.

712 Fig. 6. Spatio-temporal change in urban land use across the study area

713 Fig. 7. Decadal change in urban land cover types across the study area catchments.

714 Fig. 8. Comparison of catchment imperviousness estimated from aerial photography ( $\%IMP$ ) and  
715 topographic map-derived index of urban extent ( $URBEXT$ ) within the six catchments, for years  
716 1990, 2000 and 2010. Fig. 9. Change in impervious cover determined using two methods across  
717 the six study catchments (1960–2010).

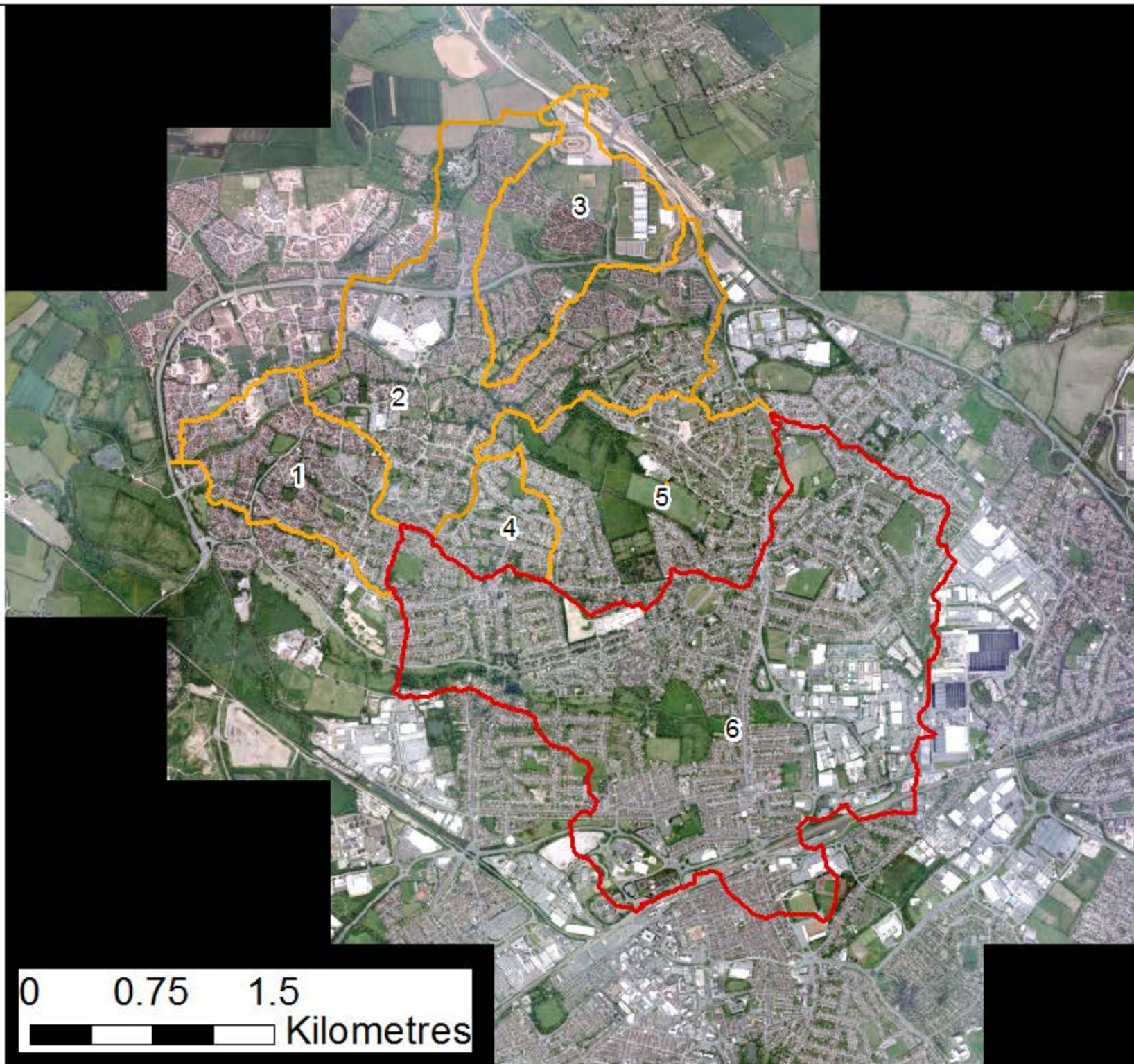
718 Fig. 10. A comparison of impervious surface maps obtained using the two methods.



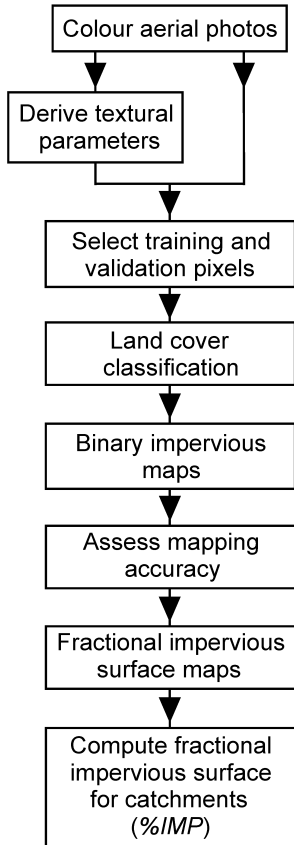
### Catchment

 Haydon Wick

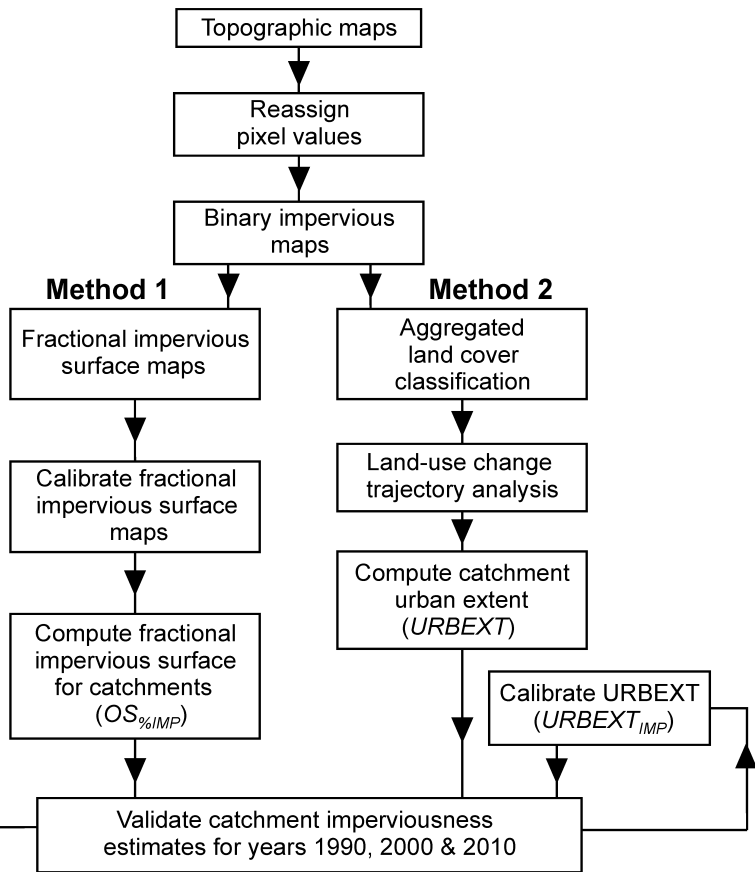
 Rodbourne



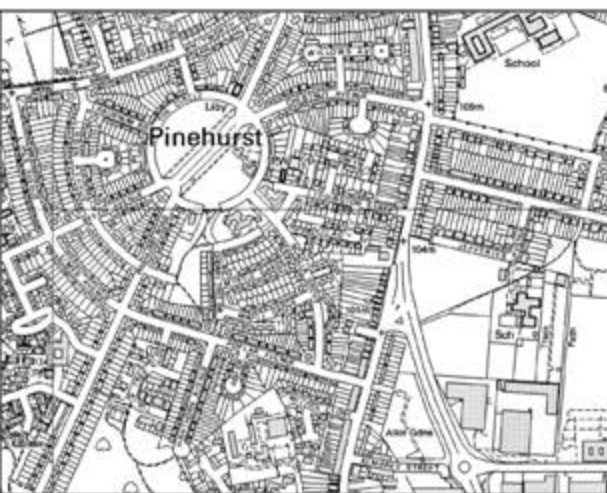
## Mapping using aerial photographs



## Mapping using topographic maps



Method 1: Fractional  
impervious surface  
mapping ( $OS_{\%IMP}$ )



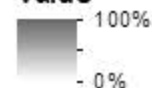
Binary 1 m raster



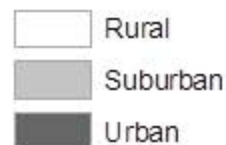
50 m grid cell

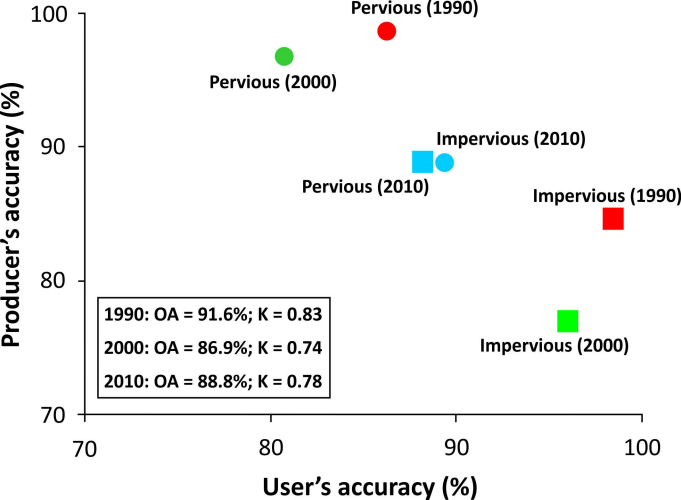
Percentage Impervious (%)

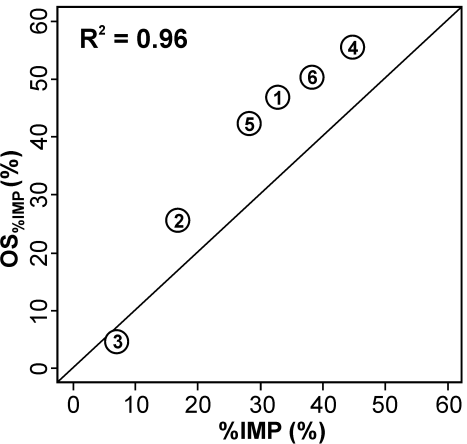
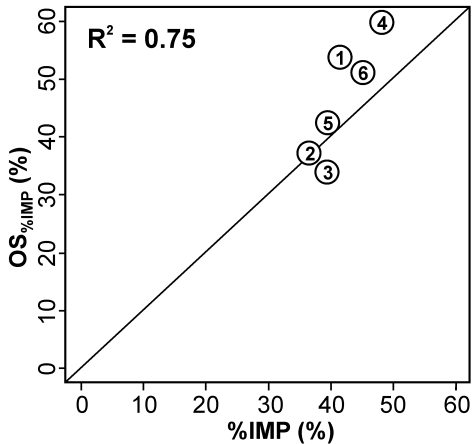
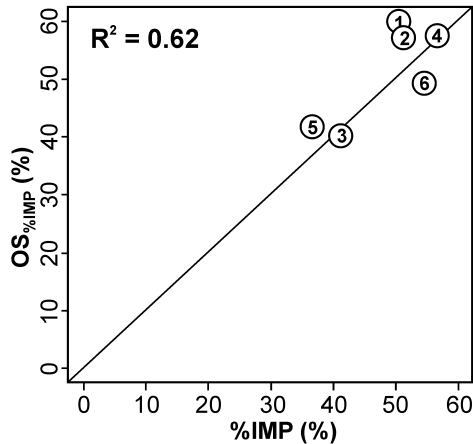
Value

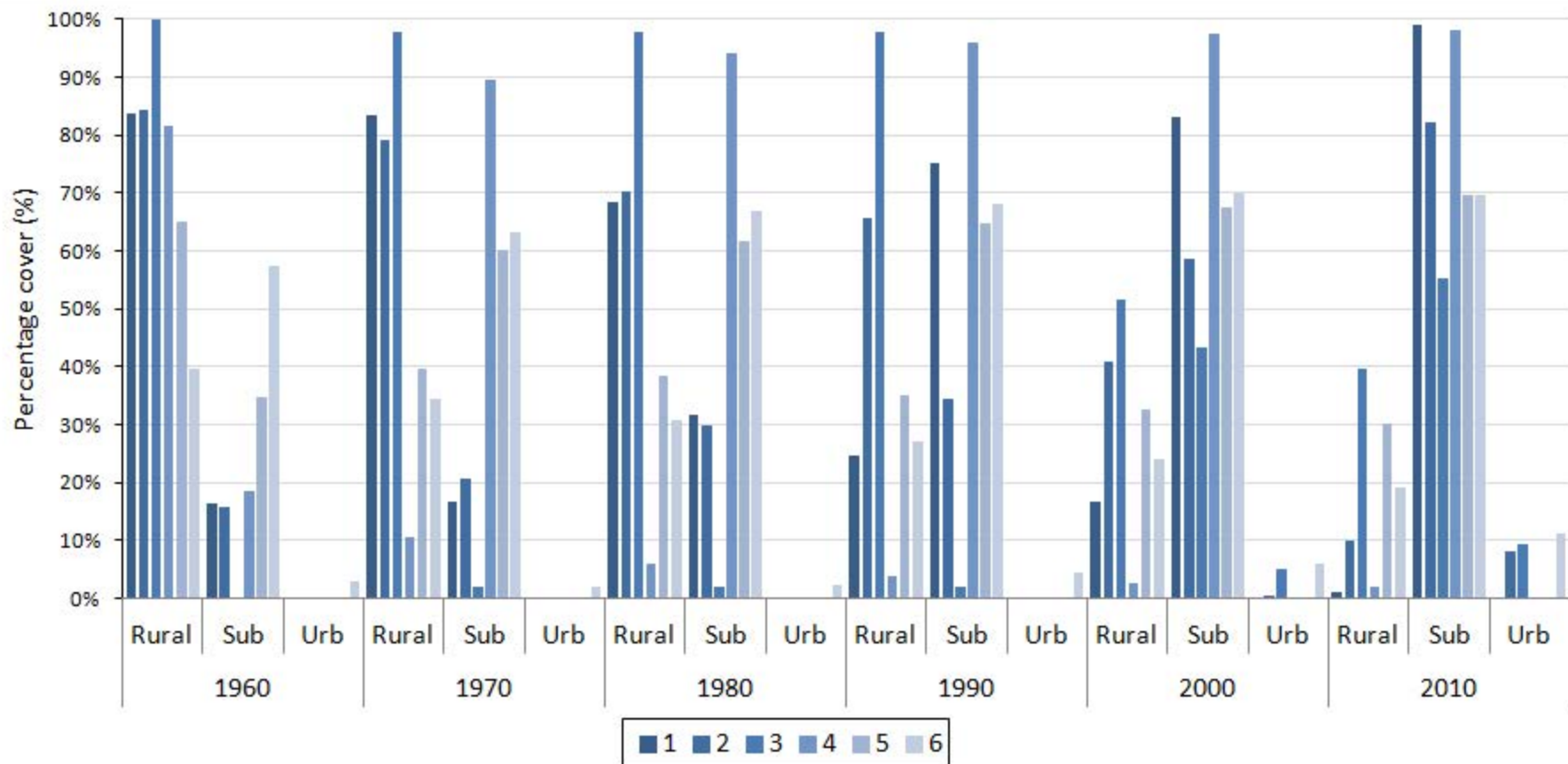


Method 2: Aggregated  
urban land-use  
classification

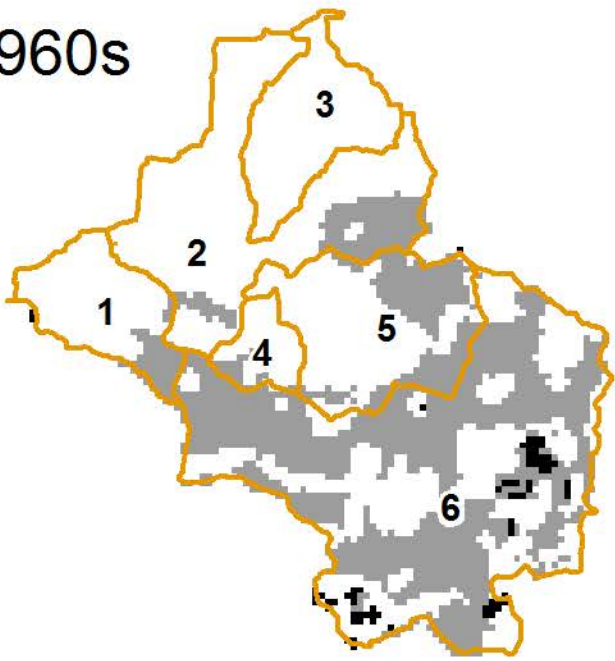




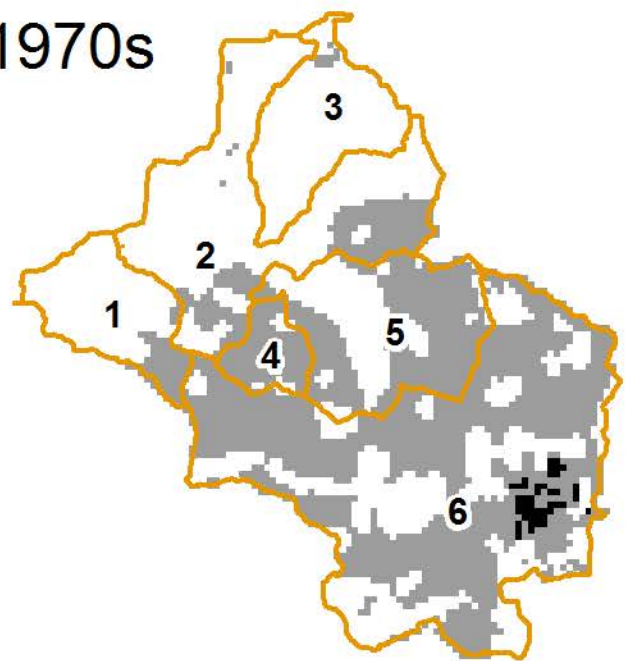
**1990****2000****2010**



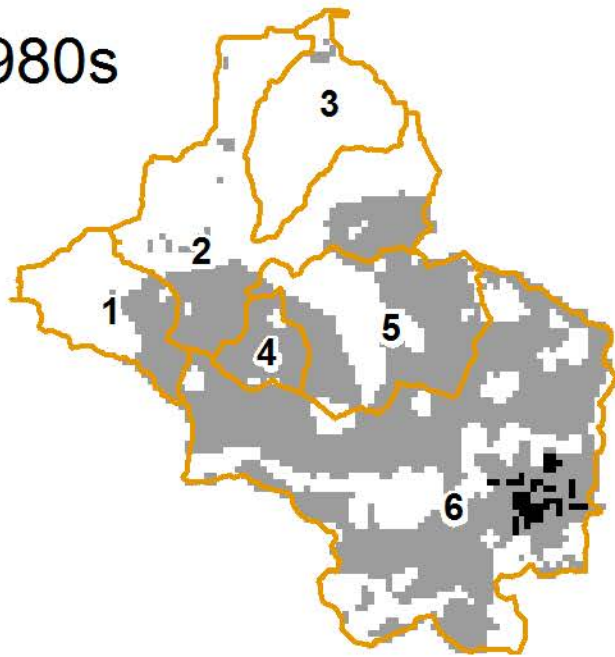
1960s



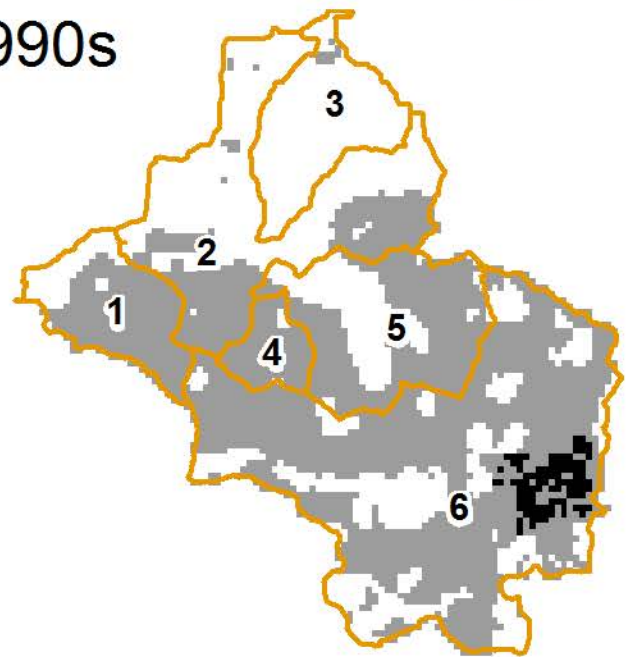
1970s



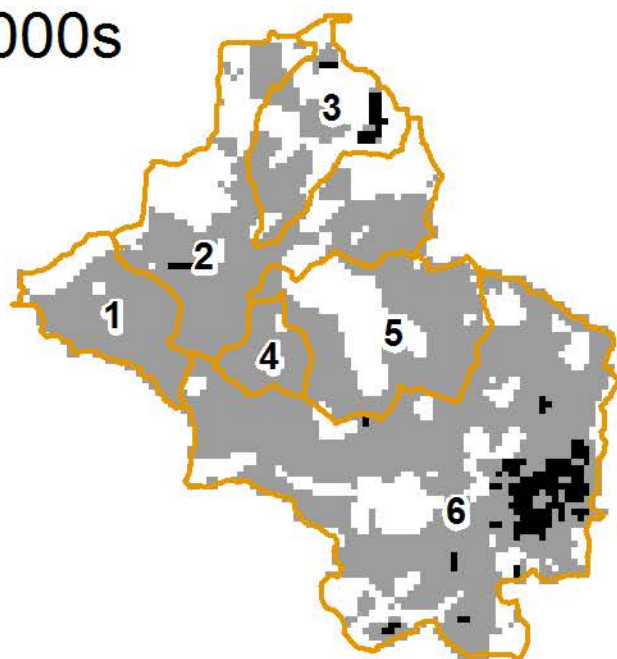
1980s



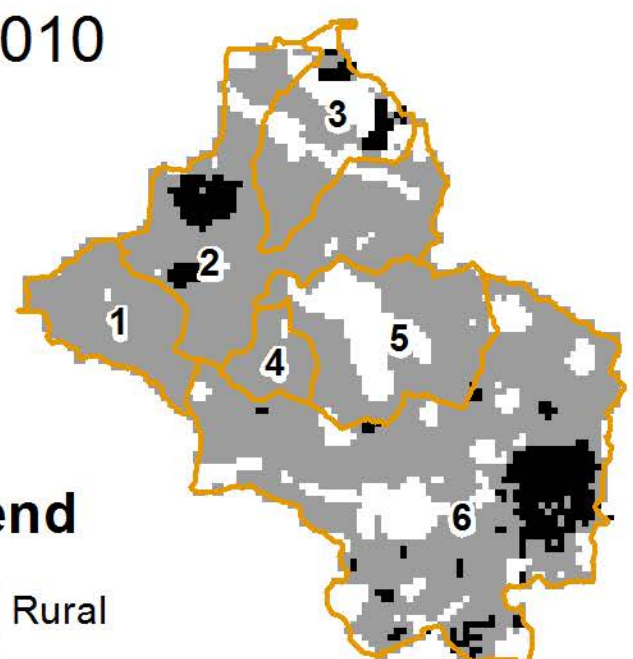
1990s



2000s



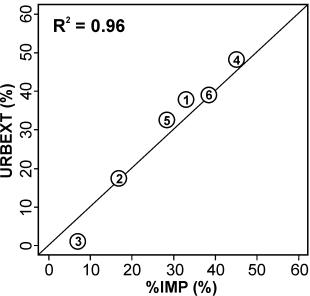
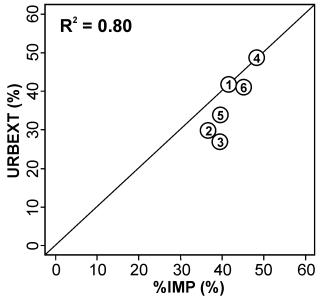
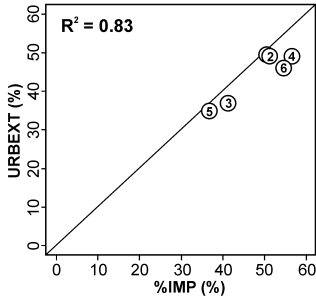
2010

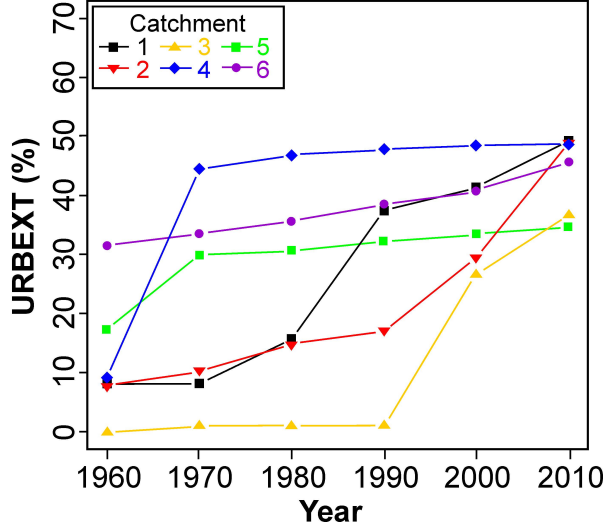
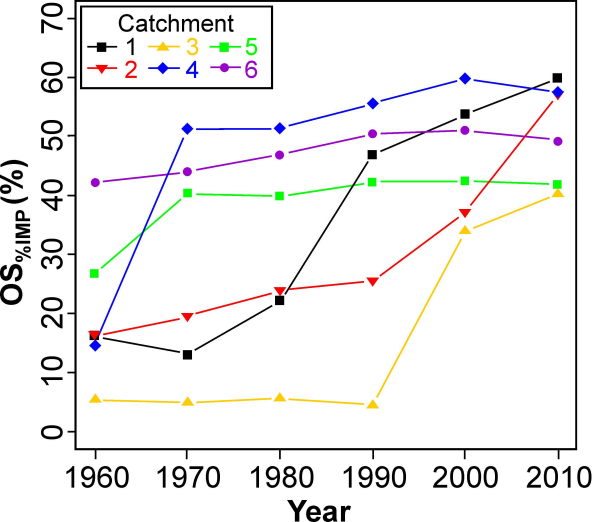


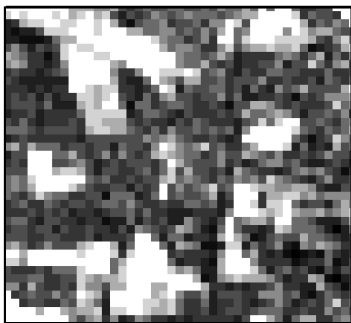
### Legend

- Rural
- Suburban
- Urban

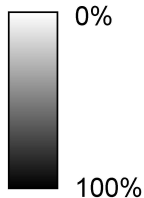


**1990****2000****2010**

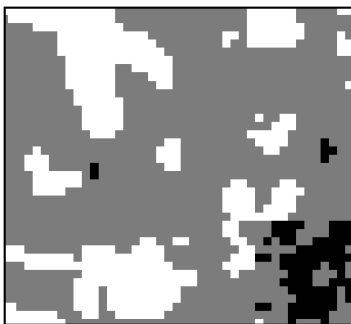
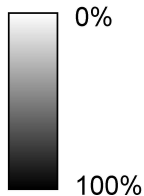




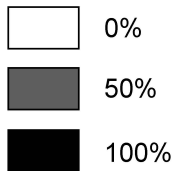
**Aerial photography  
-derived fractional  
imperviousness**



**Method 1:  
Fractional  
imperviousness**



**Method 2:  
Imperviousness**



1 km